Review of Discrete Fourier Transform During Dynamic Phasor Estimation and the Design of Synchrophasor Units

Sai Lakshmi Chukkaluru and **Shaik Affijulla**[†], Non-members

ABSTRACT

In a large and complex interconnected power system, the measurement of synchronized bus voltage and line current plays a vital role in the monitoring and precise control of various sophisticated electrical equipment for secure and reliable operation. Phasor measurement units (PMUs) are incorporated into a wide area of the power system to extract the different signals of synchronized phasors. In this paper, the capacity of the PMU phasor estimation algorithm is explored based on discrete Fourier transform (DFT) under different sampling frequency rates during various dynamic scenarios in accordance with the IEEE C37.118.1a-2014 standard. Furthermore, the performance of the DFT algorithm varies according to the phase angle and dynamic parameters such as frequency, frequency ramp rates, modulation frequency, harmonic levels, step change, decaying dc, and noise levels. The simulation results reveal that accuracy of the phasor estimation algorithm based on DFT can be achieved at high sampling frequency rates. Furthermore, the results of DFT-based phasor estimation are compared with Shank's estimation method (SEM) and the least-squares estimation method (LEM). The presented method is best suited to PMU algorithms development based on DFT for better visualization of the smart electric grid.

Keywords: Discrete Fourier Transform, DFT, Dynamic Phasor Estimation, Phasor Measurement Unit

1. INTRODUCTION

Since the 1880s, electricity generation has mainly depended on conventional energy sources, but these are currently being exhausting at a rapid rate [1]. Nowadays, due to advancements in research and technology, renewable energy sources (RES) are emerging as alternatives for providing a reliable electric power supply in response to growing demand [2]. With the integration of RES, peculiar dynamics are being exhibited by the complex interconnected power system. Traditionally, power system monitoring and control actions are performed through supervisory control and data acquisition (SCADA) systems by utilizing remote terminal units (RTU) installed at the substation to measure the magnitude of voltage and current signals. The measurements carried through RTU are not time-synchronized, limiting the precise state estimation of the SCADA system and potentially leading to lagging/incorrect monitoring of the system state rather than the actual state during dynamic scenarios in the power system [3].

To resolve the issue of precise measurement, the RTUs are replaced by phasor measurement units (PMUs), providing a global positioning system (GPS), time-synchronized accurate bus voltage, and line current phasors in the large interconnected electrical grid. Thus, the incorporation of PMU can facilitate the wide-area monitoring of a modern power system equipped with RES and power electronics for sophisticated and smooth control [4]. The utilization of various power conversion devices (e.g., switch mode power supply), intermittent loads, environmental abnormalities, and protective actions may lead to harmonics, noise, direct current (dc) components, modulating signals, high-frequency transients, etc., turning the sinusoidal signal into a non-stationary/non-sinusoidal signal in the power system.

Under these dynamic scenarios, the PMU estimation algorithm is required to accurately estimate the phasor information of corrupted electrical (voltage/current) signals as per the IEEE synchrophasor standard [5, 6]. The main idea of the standard is to provide accuracy criteria for the power system monitoring of synchrophasor measurements under different dynamic scenarios. This standard defines synchrophasor, frequency, and rate of change of frequency (RoCoF) measurement requirements and their compliance under power system operating conditions. The IEEE C37.118.1a-2014 standard is an updated version of IEEE C37.118.1-2011. For power system and control applications, several phasor estimation techniques are suggested in the literature, some of which are discussed in [7–22].

The discrete Fourier transform (DFT) estimation technique is the basic, simplest, and most popular algorithm for phasor computation. The author in [7] presents a compensation method based on frequency tracking to extract the accurate amplitude and power measurement through the DFT algorithm for online purposes. In [8], a simple zero-crossing detection-based time domain analysis is used to extract the frequency and phase of the

Manuscript received on April 9, 2022; revised on April 30, 2022; accepted on May 11, 2022. This paper was recommended by Associate Editor Kaan Kerdchuen.

The authors are with the Department of Electrical Engineering, National Institute of Technology Meghalaya, Shillong, India.

[†]Corresponding author: shaik.affijulla@nitm.ac.in

Digital Object Identifier: 10.37936/ecti-eec.2023211.248548

signal. However, it is slow and unreliable for disturbance signals.

In [9], the modulated sliding DFT (MSDFT) algorithm with Taylor's series expansion is used to reduce the computational burden, providing better accuracy than DFT and sliding DFT algorithms during phasor measurement applications. Several signal processing methods are based on the time-frequency domain (TFD) analysis. These include short-term Fourier transform (STFT) for low computationally enhanced parameter estimation in low-cost, real-time signal processing [10] and the fast Taylor weighted least square algorithm to accurately estimate the real-time synchronized signal [11]. This algorithm estimates the signal phasor at runtime by applying discrete-time Fourier transform (DTFT) twice at the nominal frequency with some elementary arithmetic operations.

Furthermore, in [12], the windowing effect on the real-value Taylor-based weighted least square (TWLS) algorithm is analyzed during noisy scenarios with constant amplitude and phase, where the Taylor's series of the signal is truncated to second. A simple algorithm based on Teage's energy operator is suggested to compute the amplitude, phase, frequency, and RoCoF of the power signal with a high sampling rate [13].

The author in [14] introduces an adaptable sampling frequency-based estimation technique which is faster than zero-crossing, detection-based estimation, although it is less popular. In [15], adaptive notch filtering is implemented using a cluster of notch filters to obtain the fundamental components of a signal. An enhanced phase-locked loop (PLL) is designed in [16] using a phase detector (PD) to obtain the phase error with a single frequency term. In [17], a space vector (SV) approach is implemented to obtain positive sequence data for a synchrophasor to estimate the signal frequency.

The author in [18] discusses an algorithm to estimate the dynamic phasors based on self-convolution and Hilbert transform concepts, in which self-convolution and Hilbert transform operations are utilized for magnitude and phase angle estimation, respectively. A low-cost dictionary-based phasor estimation technique suitable for protection class PMUs has been recently suggested in [19].

In [20], a new measurement class distribution-level PMU technique based on empirical wavelet transform (EWT), together with a hybrid frequency estimator, is suggested to estimate the phasors of fundamental and harmonic components in a distribution-level signal. An adaptive wavelet transform (AWT) method is introduced in [21], which adapts itself according to the frequency drift during off-nominal frequency events in the power system.

Moreover, the authors in [22] present a simple and effective test algorithm to validate the adaptation of PMU according to the IEEE C37.118.1a 2014 standard, further discussing the concept of total vector error (TVE) and compliance tests, and defining the variation in frequency and RoCoF, its error limits for steady-state, and the dynamic conditions of the power system.

***Table 1**: Summary of commercial ADCs.*

N (spc)	Sample rate (sps)	Min cost (rpu)	Max cost (rpu)	Resolution (bit)
64	3300*	84	230	16
128	6400	1000	1540	32
256	14000*	170	600	16
2048	105000*	1000	1500	32

Generally, DFT is utilized to extract the fundamental phasor through the positive sequence components of a three-phase signal. The DFT-based phasor estimation technique is a frequency dominant method. Due to non-integer harmonics and decaying dc components, the Fourier spectrum of non-sinusoidal/non-stationary signals may exhibit frequency leakage, leading to inaccurate fundamental phasor estimation.

Furthermore, the scalloping loss (i.e., associated with the main lobe of window performance of DFT) may occur in the Fourier spectrum of a signal during modulation (low frequency) and frequency ramp scenarios, leading to inaccurate fundamental phasor estimation. To avoid spectral leakage and the averaging effect, a considerable number of samples (i.e., high sampling rate in the order of 10^2 kHz) is required to enhance the accuracy of DFT-based phasor estimation algorithms during dynamic scenarios.

The sampling rate of signal demands for costly analog to digital converters (ADC) is high. The costs of various ADC manufactured by Texas Instruments Ltd., about 50 Hz in frequency, are presented in Table 1. N denotes the number of samples per cycle (spc), i.e., 20 ms, sps denoted the number of samples per second where * indicates the commercially available sampling rate of Texas Instruments ADCs and rpu denotes the rupees per unit.

Thus, the objective of this current study is to explore the capacity of DFT during the fundamental phasor estimation of a non-sinusoidal/non-stationary signal under different sampling frequency rates, i.e., $N \in \{64, 128, 256, 2048\}$. This paper makes the following contribution to the existing literature:

- An in-depth analysis of dynamic phasor estimation based on DFT with various ADC sampling rates.
- Discrete Fourier transform was tested under all test signals according to the IEEE C37.118.1a 2014 standard under in-depth analysis to support the development of modern PMUs for the wide-area monitoring of power systems.
- The results are compared with other existing phasor estimation techniques, viz., SEM [23], and LEM [24].

The remainder of the paper is organized as follows. The theory of the DFT based phasor estimation process is presented in Section 2. The simulation results with

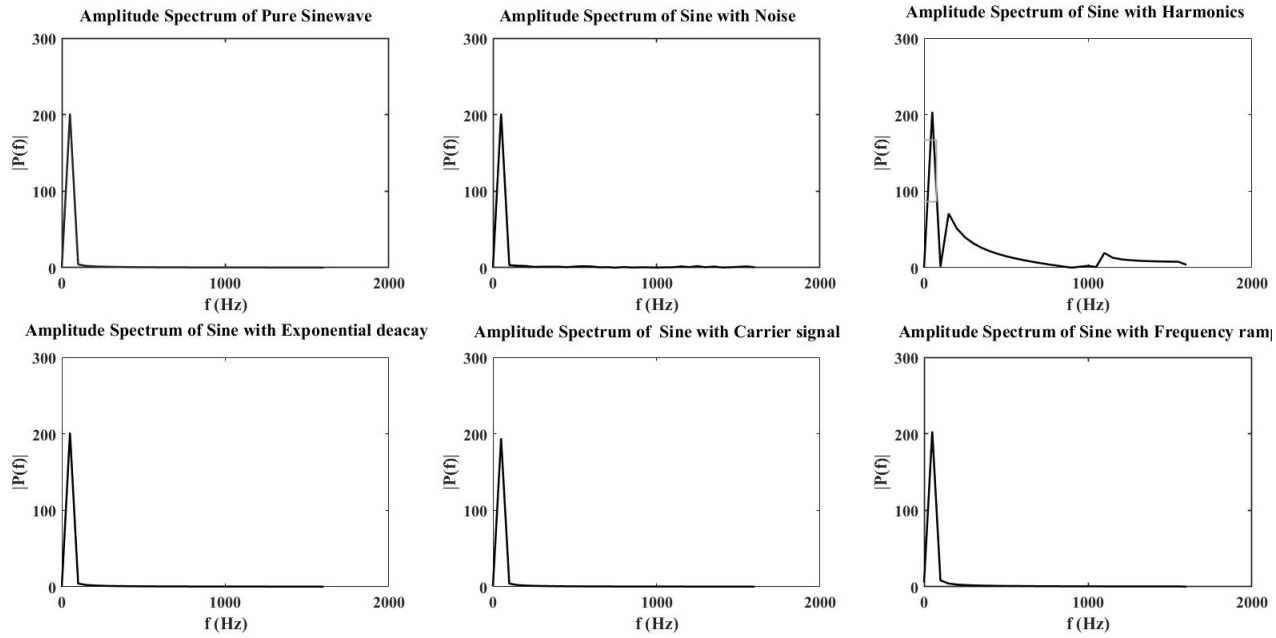

***Fig. 1**: Phase response of test signals according to the IEEE C37.118.1a-2014 standard.*

the DFT based estimator during various dynamic signals are discussed according to IEEE C37.118.1a-2014, while its capacities are explored in Section 3. Finally, the conclusion of the work is presented in Section 4.

2. THEORY OF FOURIER TRANSFORM FOR PHASOR ESTIMATION

In this paper, traditional DFT is utilized to compute the phasor of a signal (i.e., voltage/current). DFT characteristics under various sampling frequency (f_s) of a signal Eq. (1) are explored during different abnormal scenarios.

Let the steady-state voltage/current signal, i.e., $q(t)$, be mathematically expressed as

$$q(t) = Q_m \sin(2\pi f_0 t + \theta) \tag{1}$$

where Q_m is signal magnitude and f_0 is signal frequency in hertz (Hz), t is time in second (s) and θ is signal phase angle in radian (rad).

On the digitalization of Eq. (1) with N number of samples per cycle (i.e., for a period of $T = 1/f_0$) by sampling frequency ($f_s = N f_0$) as

$$q[n] = Q_m \sin(kn + \theta) \tag{2}$$

where $q[n]$ is the discrete signal of $q(t)$, $k = 2\pi/N$ which is a constant, n varies from 0, 1, 2, 3, ..., $(N-1)$.

2.1 Application of DFT

The DFT is applied to signal in Eq. (2) and mathematically expressed as

$$Q[\omega] = \frac{\sqrt{2}}{N} \sum_{n=0}^{N-1} q[n] e^{\frac{-j2\pi n\omega}{N}} \tag{3}$$

where $Q[\omega]$ is the discrete Fourier transform (DFT) of Eq. (2), $\omega = 2\pi f$ is angular frequency in rad/s.

By simplifying Eq. (3) using Eq. (2) as

$$Q[\omega] = \frac{\sqrt{2}Q_m}{N} \sum_{n=0}^{N-1} \sin(kn + \theta) \left(\cos(kn\omega) - j \sin(kn\omega)\right) \tag{4}$$

Let $A = kn + \theta$ and $B = kn\omega$, which simplifies Eq. (4) as

$$Q[\omega] = \frac{jQ_m}{\sqrt{2}N} \sum_{n=0}^{N-1} \left(e^{-j(A+B)} - e^{j(A-B)}\right) \tag{5}$$

Thus, the frequency (ω) distribution i.e., DFT of given signal Eq. (2) can be computed as

$$Q[\omega] = \frac{jQ_m}{\sqrt{2}N} \sum_{n=0}^{N-1} \left(e^{-j[kn(1+\omega)+\theta]} - e^{j[kn(1-\omega)+\theta]}\right) \tag{6}$$

The frequency domain and amplitude spectrum of the Fourier transform computed signals are plotted in Fig. 1. It can be observed that for each IEEE C37.118.1a-2014 standard signal, the fundamental magnitude is located at the 50 Hz frequency component only.

2.2 Extraction of fundamental signal phasor

During power system operation and control, the fundamental phasor information of voltage/current signal(s) plays a vital role in decision-making and allows suitable corrective actions to be taken to retain the system

operating state within the stable region. From Eq. (6), the signal fundamental phasor (i.e., $\omega = 1$) can be extracted as

$$Q[1] = \frac{jQ_m}{\sqrt{2}N}\sum_{n=0}^{N-1} e^{-j(2kn+\theta)} - \frac{jQ_m}{\sqrt{2}N}\sum_{n=0}^{N-1} e^{j\theta} \quad (7)$$

On substitution of the k value and expansion, Eq. (7) gives

$$Q[1] = \frac{jQ_m}{\sqrt{2}N}\left[\sum_{n=0}^{N-1}\cos\frac{4\pi n}{N}\cos\theta - \sum_{n=0}^{N-1}\sin\frac{4\pi n}{N}\sin\theta\cdots - j\left(\sum_{n=0}^{N-1}\sin\frac{4\pi n}{N}\cos\theta - \sum_{n=0}^{N-1}\cos\frac{4\pi n}{N}\sin\theta\cdots\right)\right] - \frac{jQ_m}{\sqrt{2}N}\sum_{n=0}^{N-1} e^{j\theta} \quad (8)$$

From trigonometric identities, the sum of sine and cosine terms in Eq. (8) are equal to "zero" and simplified Eq. (8) as

$$Q[1] = -\frac{jQ_m e^{j\theta}}{\sqrt{2}} \quad (9)$$

$$Q[1] = -\frac{jQ_m(\cos\theta + j\sin\theta)}{\sqrt{2}} \quad (10)$$

$$Q[1] = Q^*\angle\theta^* \quad (11)$$

where $Q_m = \sqrt{2}Q^*$, $\theta = \theta^* + 90°$, Q^* and θ^* are estimated fundamental magnitude and phase angle of the given signal Eq. (1) by DFT.

The expressions Eqs. (9), (10), and (11) reveal that the magnitude of signals estimated by the DFT-based phasor estimation is independent of the total number of samples (N). However, in this paper, the fundamental phasor estimation of a given signal by DFT under various sampling frequencies (i.e., varied N) during different dynamic scenarios has been explored and DFT capacity discussed in the results section.

3. SIMULATION RESULTS

The efficacy of DFT to compute fundamental phasor with a varied sampling frequency (f_s) is revealed under different dynamic conditions according to the IEEE C37.118.1a-2014 Standard [5]. The DFT-based phasor estimation algorithm was developed using MATLAB software in an Intel® Core™ i5-8300H processor at 2.30 GHz on a personal computer. To evaluate the performance of DFT-based phasor estimation algorithm, a performance parameter called total vector error (TVE) is utilized and defined as

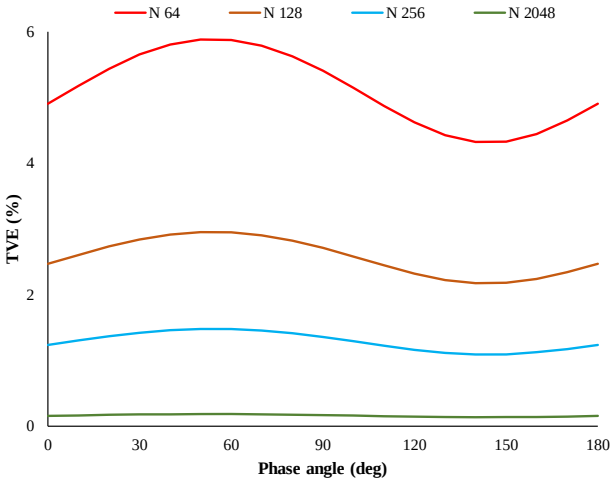

Fig. 2: TVE response during the change in phase of a pure sinusoidal signal.

$$\%\,\text{TVE} = \sqrt{\frac{(S_r^a - S_r^e)^2 + (S_i^a - S_i^e)^2}{(S_r^a)^2 + (S_i^a)^2}} \times 100 \quad (12)$$

where S_r^a, S_r^e and S_i^a, S_i^e are real and imaginary parts of actual and estimated phasors, respectively.

During all simulations, the following parameter values are considered: Q_m as 200 V, f_0 as 50 Hz, θ as 0°, a phasor reporting rate of 50, estimation window length of 20 ms for 50 Hz signal, and simulation time (t) of 1.5 s.

Additionally, DFT-based phasor estimation with a sampling frequency of 2048 is compared with other phasor techniques, i.e., Shank's estimation method (SEM) and least-squares estimation method (LEM) with a sampling frequency of 128.

3.1 Signal without any Abnormality

In the power system, the interconnected alternators can deliver grid power at stable voltage, i.e., sinusoidal wave without exception (fundamental quantity) due to the symmetrical structure and balanced operation. The fundamental sinusoidal signal can be represented mathematically as

$$q_1(t) = Q_m \sin\left(2\pi f_0 t + \theta\right) \quad (13)$$

The signal in Eq. (13) is provided to the DFT-based phasor estimation algorithm to compute the absolute magnitude and phase angle. The caliber of DFT is tested by varying the phase angle (θ) from 0° to 180° in steps of 10° with a constant magnitude (Q_m) under different sampling frequencies, i.e., $N \in \{64, 128, 256, 2048\}$. The performance of DFT in computing the fundamental phasor in terms of TVE is shown in Fig. 2. Furthermore, the DFT-based phasor estimation algorithm is performed in time (t) with different sampling frequencies, i.e., $N \in \{64, 128, 256, 2048\}$ and its efficiency is shown in Fig. 3.

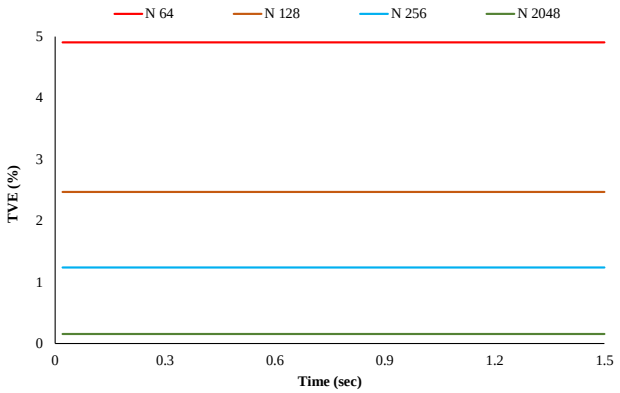

Fig. 3: *TVE response of sinusoidal signal at $\theta = 0^\circ$ and $Q_m = 200\,V$.*

Table 2: *Effect of sample rate on pure sinusoidal signal.*

N	% TVE		
	Maximum	Minimum	Mean
64	5.8819	4.3198	5.1216
128	2.9521	2.1738	2.5733
256	1.4788	1.0903	1.2897
2048	0.1852	0.1366	0.1615

The maximum, minimum, and mean TVEs are extracted from Fig. 2 and presented in Table 2.

Fig. 2 and Table 2 show that under lower sampling frequencies, i.e., $N < 128$, the TVE varies with a change in phase angle, i.e., maximum at 60°, otherwise, there is no impact on the variation of TVE, i.e., it is almost constant. Furthermore, Fig. 3 reveals that the estimation accuracy of the phasor increases along with the sampling frequency, i.e., the minimum N should be 2048 to attain a TVE accuracy of 0.1553%.

3.2 Signal with an Abnormality in Frequency

3.2.1 Off-nominal frequency event

The interconnected alternators in the power system operate at a nominal frequency, i.e., (f_0), for a given load scenario. Due to the dynamics in load demand, the frequency at which the power developed by the alternator deviates from its nominal frequency, known as off-nominal frequency (f), the signal with off-nominal frequency, can be represented mathematically as

$$q_2(t) = Q_m \sin(2\pi f t + \theta) \tag{14}$$

where $f = f_0 + \Delta f$, Δf is the frequency deviation in Hz.

To verify the performance of the DFT-based phasor estimation, the signal in Eq. (14) is provided to extract the absolute magnitude and phase angle. The value of DFT in terms of TVE is computed by varying Δf from −0.5 Hz to 0.5 Hz in steps of 0.01 Hz with a fixed magnitude (Q_m) under different sampling frequencies, i.e., $N \in \{64, 128, 256, 2048\}$. The efficacy with which DFT can extract the fundamental phasor in terms of TVE during off-nominal frequencies is depicted in Fig. 4.

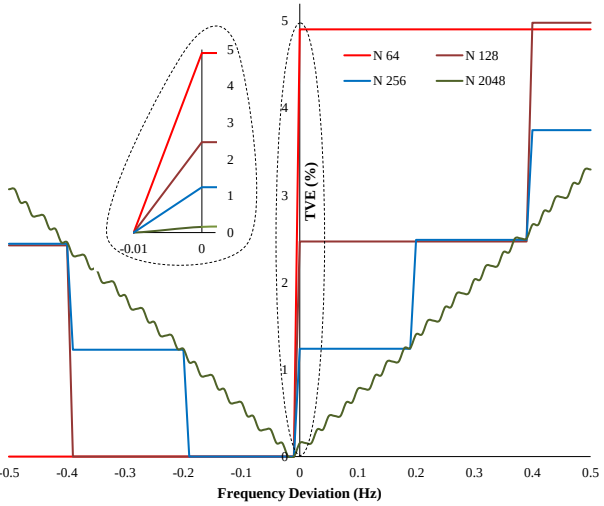

Fig. 4: *TVE response during change in frequency of a pure sinusoidal signal.*

From Fig. 4, it can be observed that TVE rises with a slope almost equal to 490%/Hz until $\Delta f = 0$ Hz from −0.01 Hz (i.e., $f = 49.9$ Hz), zero for all $\Delta f < -0.01$ Hz, 4.9055% during $0 < \Delta f < \pm 0.78$ Hz and 9.8205% for all $\Delta f > \pm 0.78$ Hz under N as 64 spc. Moreover, the TVE rises with a slope almost equal to 247%/Hz from $\Delta f = -0.01$ Hz to 0 Hz, a change in TVE from 2.4691% to 4.9814% occurs between $\Delta f = 0.39$ Hz and 0.4 Hz with a slope of 251%/Hz and a subsequent 2.5123% step change in TVE at intervals of 0.4 Hz during the 128 spc scenario.

Furthermore, a staircase TVE response is exhibited with a slope of 123%/Hz, 15%/Hz, and a step change interval of 0.2 Hz, 0.025 Hz with a maximum TVE of 1.2386%, 0.1552% during 256 spc and 2048 spc scenarios, respectively. Thus, the TVE response is like a staircase in nature with a step size of $0.8/k$ during phasor estimation in the event of frequency deviation under a specified sampling rate, i.e., $N = 2^{(6+k)}$. The value of k limits the maximum TVE under frequency deviations ranging from −0.5 Hz to 0.5 Hz during DFT-based phasor estimation.

Fig. 5 indicates that the TVE response is less than 3.0% for Eq. (14) within the frequency deviation range of ±0.5 Hz with DFT-based phasor estimation, whereas, with Shank's estimation method (SEM), the TVE is 4.8%, while for the LEM it is 8.4%.

3.2.2 Frequency ramp event

The frequency parameter must be maintained within a tolerance level (i.e., ±5% Hz) to secure the complex interconnected power system. An automatic load frequency control (ALFC) mechanism is incorporated at the alternator terminals to retain system frequency within the tolerance level. Due to the multi-valve operation of an alternator, the frequency increases with respect to time as a ramp, mathematically represented as

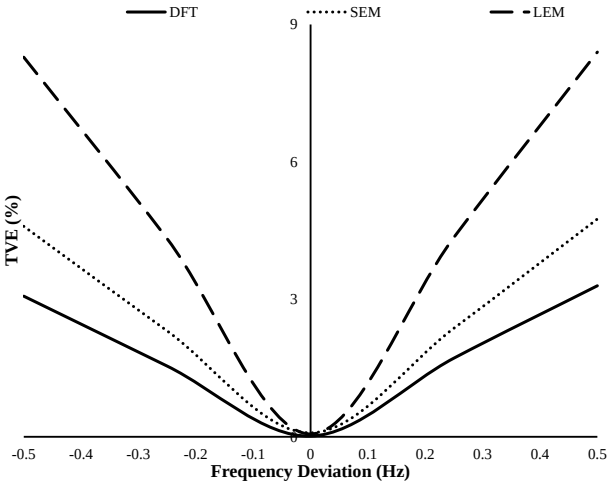

Fig. 5: *TVE response of Eq. (14) with DFT, SEM, and LEM phasor estimation techniques.*

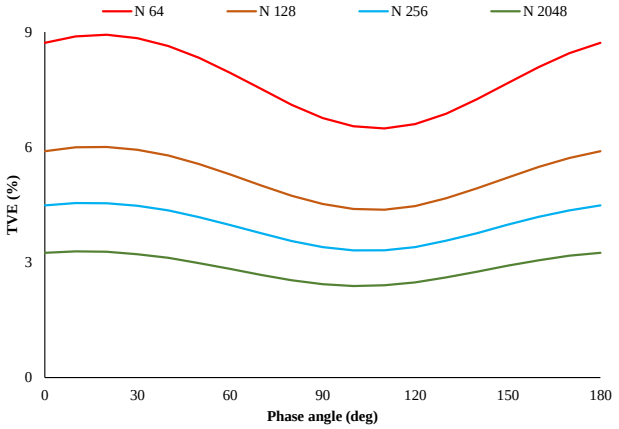

Fig. 6: *TVE response during the change in phase of Eq. (15) under a positive frequency ramp.*

$$q_3(t) = Q_m \sin\left(2\pi f_0 t \pm \pi P_f t^2 + \theta\right) \qquad (15)$$

where P_f is the frequency ramp rate in Hz/s.

The signal in Eq. (15) is provided to the DFT-based phasor estimation algorithm under the frequency ramp rate, i.e., (P_f) of +1 Hz/s and −1 Hz/s. To showcase its capacity, the phase angle (θ) is varied from 0° to 180° in steps of 10° at a constant magnitude (Q_m) under different sampling frequency, i.e., $N \in \{64, 128, 256, 2048\}$.

For better impact, a period, i.e., 20 ms from $t = 0.36$ s to $t = 0.38$ s of the signal is considered to reveal the TVE efficacy under positive and negative frequency ramps, as shown in Figs. 6 and 8, respectively. Furthermore, the efficiency of the DFT-based phasor estimation algorithm is evaluated with respect to time under positive and negative frequency ramps during different sampling frequencies, i.e., $N \in \{64, 128, 256, 2048\}$, as depicted in Figs. 7 and 9, respectively.

As can be observed from Fig. 6, the TVE response is a sine wave with a peak, i.e., a maximum TVE at 20° and a

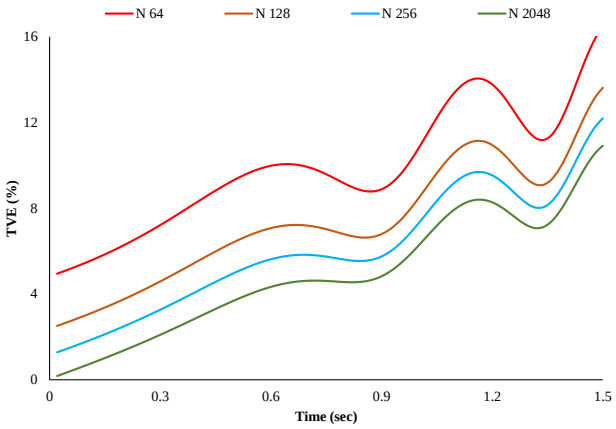

Fig. 7: *TVE response of Eq. (15) with P_f = +1 Hz/s.*

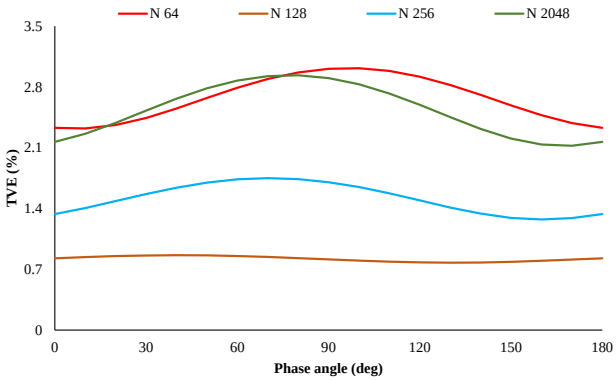

Fig. 8: *TVE response during the change in phase of Eq. (15) under a negative frequency ramp.*

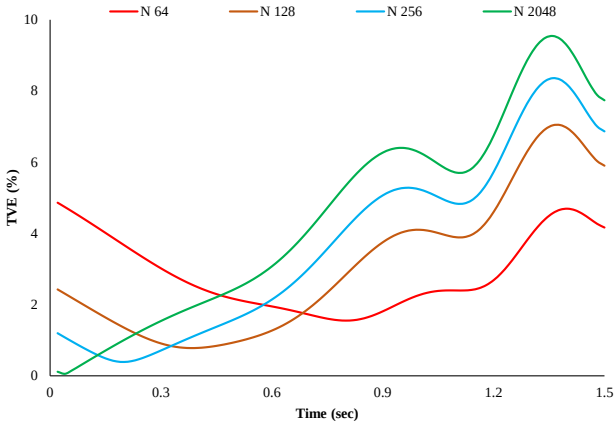

Fig. 9: *TVE response of Eq. (15) with P_f = −1 Hz/s.*

dip, i.e., minimum TVE at 110° during the change in phase angle of a positive frequency, i.e., +1 Hz/s ramp signal under different sampling frequencies. Similarly, Fig. 8 shows a maximum TVE of 3.0153%, 0.8622%, 1.7495%, and 2.9343% at 100°, 40°, 70°, 80°, during 64 spc, 128 spc, 256 spc, and 2048 spc, respectively, are observed during a change in the phase angle of negative frequency, i.e., −1 Hz/s ramp signal. Moreover, a constant TVE

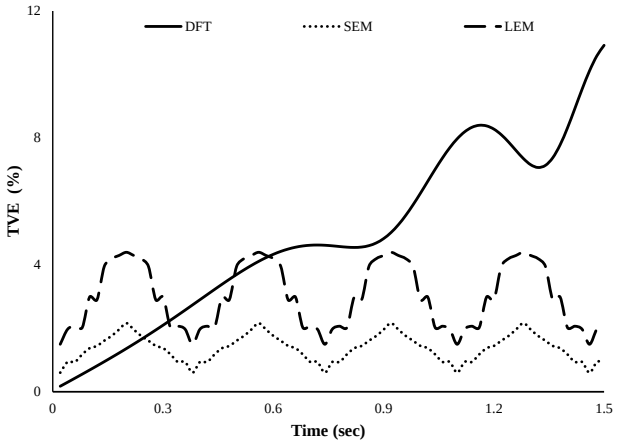

***Fig. 10**: TVE of Eq. (15) with P_f = +1 Hz/s for DFT, SEM, and LEM phasor estimation techniques.*

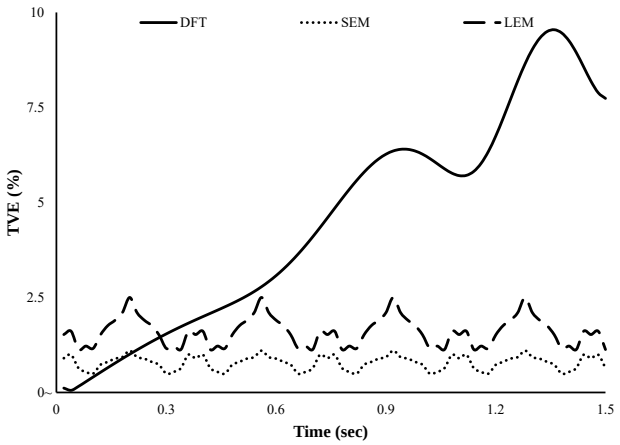

***Fig. 11**: TVE of Eq. (15) with P_f = −1 Hz/s for DFT, SEM, and LEM phasor estimation techniques.*

of 0.8200% can be observed under 128 spc during the negative frequency ramp signal phasor estimation.

As revealed by Figs. 7 and 9, the TVE response increases non-linearly over time during positive and negative frequency ramp events, irrespective of the sampling rate chosen during phasor estimation. Furthermore, the acceptable TVE, i.e., less than 3%, can be achieved for a maximum duration of 0.4 s and 0.9 s during +1 Hz/s and −1 Hz/s ramp rates with a sampling rate of 0.40 s and 0.58 s during +1 Hz/s and −1 Hz/s ramp rates, respectively, with a sampling rate of $N = 2048$ spc.

In addition, Figs. 10 and 11 reveal that the TVE response increases progressively with time for Eq. (15) with the DFT-based phasor estimation whereas the TVE response of the SEM and LEM are periodic in nature with sustained oscillatory behavior.

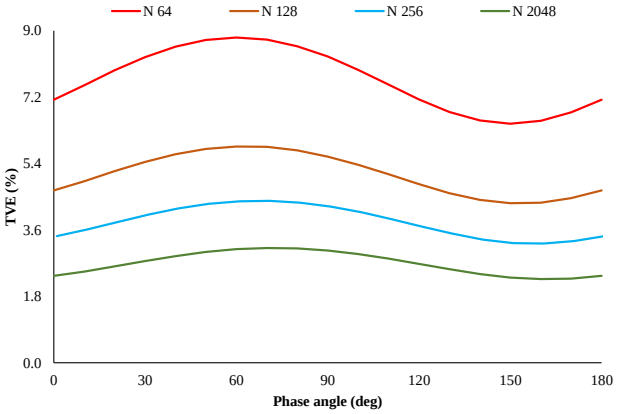

***Fig. 12**: TVE response during the change in phase of Eq. (16) under a modulation event.*

***Table 3**: Effect of sample rate during modulation.*

N	Mean %TVE	Nature
64	4.9377	Sine
128	2.5517	Sine
256	1.6808	Distorted Sine
2048	1.4051	Distorted Sine

3.3 Signal with an Abnormality in Waveform

3.3.1 Modulation event

During abnormal scenarios such as balanced or unbalanced faults, overloaded transmission lines, and generator outages, the power system may experience power oscillations, i.e., power swings. These power swings can be represented as amplitude and phase-modulated signals mathematically expressed as

$$q_4(t) = Q_m \left[1 + K_1 \sin(2\pi f_m t)\right] \sin\left(2\pi f_0 t + K_2 \sin(2\pi f_m t) + \theta\right) \quad (16)$$

where $K_1 = 0.1$ is amplitude modulation coefficient, $K_2 = \pi/18$ is phase modulation coefficient, $f_m = 2$ Hz is the frequency of modulation.

The efficacy of the DFT-based phasor estimation algorithm during the modulation scenarios is shown in Fig. 12 by the stretching phase angle (θ) ranging from 0° to 180° with a step size of 10° at fixed magnitude (Q_m) under different sampling frequencies, i.e., $N \in \{64, 128, 256, 2048\}$. Furthermore, the DFT strength during phasor estimation of Eq. (16) is depicted in Fig. 13 under different sampling frequencies, i.e., $N \in \{64, 128, 256, 2048\}$ as summarized in Table 3.

Fig. 12 reveals that the difference between maximum and minimum TVE is 2.3375%, 1.5364%, 1.1572%, and 0.8413% under 64, 128, 256, and 2048 spc, respectively, with its accuracy enhancing from 0° to 180°. As can be observed from Fig. 13 and Table 3, the large TVE (> 3%)

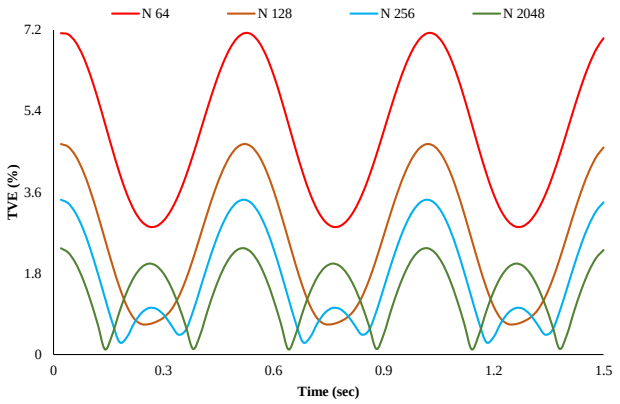

***Fig. 13**: TVE response of Eq. (16) with $f_m = 2\,Hz$.*

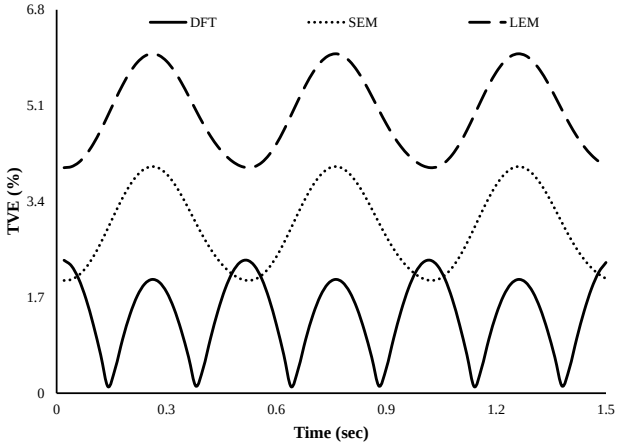

***Fig. 14**: TVE response of Eq. (16) with DFT, SEM, and LEM phasor estimation techniques.*

is sinusoidal in nature with a period of $1/f_m$, i.e., 0.5 s under low sampling frequencies, i.e., $N \in \{64, 128\}$. Furthermore, the improved TVE (< 3%) is achieved with the distorted sine of $1/f_m$, i.e., 0.5 s during high sampling frequencies, i.e., $N \in \{256, 2048\}$.

Fig. 14 reveals that the TVE response distorts the sine wave over time for Eq. (16) with DFT-based phasor estimation, whereas with SEM and LEM, the TVE response is sinusoidal in nature.

3.3.2 Harmonic event

A large interconnected power system demands flexible operation to meet the economic requirements of the energy management center. Power system flexibility can be achieved by utilizing electronic converters, which inject voltage and current harmonics into consumer and utility levels. The signal with harmonics is mathematically represented as

$$q_5(t) = Q_m \sin\left(2\pi f_0 t + \theta\right) + \sum_{k=3}^{21} Y_k \sin\left(2\pi f_k t + \theta\right) \tag{17}$$

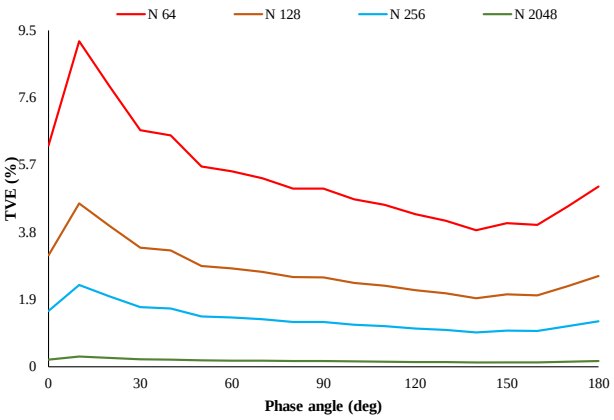

***Fig. 15**: TVE response during the change in phase of Eq. (17) under a harmonic event.*

***Table 4**: Effect of sample rate during harmonics.*

N	% TVE		
	Maximum	Minimum	Mean
64	9.1947	5.3905	3.8562
128	4.6133	2.7082	1.9359
256	2.3106	1.3572	0.9698
2048	0.2892	0.1700	0.1214

where k is the order of harmonics, i.e., 3^{rd} to 21^{st}, Y_k is the peak amplitude of the k^{th} order harmonic signal, $f_k = kf_0$, f_0 is the fundamental/nominal frequency.

The signal in Eq. (17) is given to the DFT-based phasor estimation algorithm to showcase its capacity by changing the phase angle (θ) from 0° to 180° with a step size of 10° at a fixed magnitude (Q_m) under different sampling frequencies, i.e., $N \in \{64, 128, 256, 2048\}$, as shown in Fig. 15 and summarized in Table 4. Furthermore, the DFT's strength during the phasor estimation in Eq. (17) is depicted in Fig. 16 under different sampling frequencies, i.e., $N \in \{64, 128, 256, 2048\}$.

From Fig. 15, it can be observed that TVE reaches maximum at $\theta = 10°$ and minimum at $\theta = 140°$ irrespective of the sampling frequencies, i.e., N during phase angle variations, while the mean TVE is reduced with a large N as shown in Table 4.

The TVE response is constant in time during the phasor estimation of a signal with harmonics, while a minimum TVE of 0.165% is attained at 2048 spc. Thus, the simulation results reveal that DFT-based algorithms with high sampling rates are immune to harmonics during fundamental phasor estimation.

Fig. 17 reveals that overall, the TVE response is constant over time for Eq. (17) with DFT-based phasor estimation at a magnitude of 0.16%, whereas SEM and LEM show a TVE response of 2.32% and 4.91%, respectively.

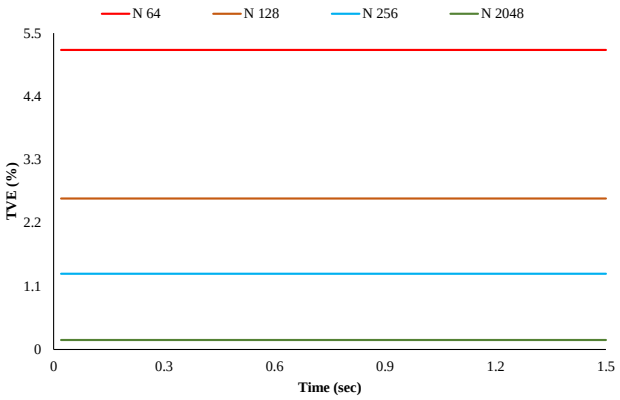

Fig. 16: *TVE response of Eq. (17) with various harmonics up to 21st order according to the IEEE C37 standard.*

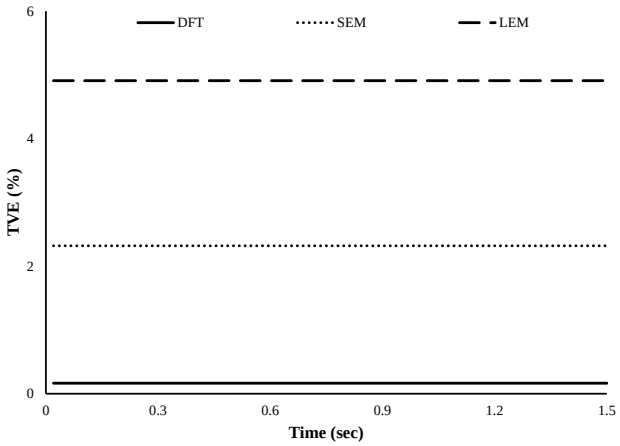

Fig. 17: *TVE response of Eq. (17) with DFT, SEM, and LEM phasor estimation techniques.*

3.4 Signal with a Parameter Abnormality

3.4.1 Step change event

During fault conditions, the magnitude and phase angle of the voltage/current signal may suddenly increase or decrease in compensation devices (capacitive banks, reactor units, etc.) These sudden deviations in step can be represented mathematically as the original signal:

$$q_6(t) = \left(Q_m + U_m(t)M_x\right)\sin\left(2\pi f_0 t + U_m(t)P_a + \theta\right) \tag{18}$$

where M_x and P_a are factors of change in magnitude and phase with 10% of the original signal, $U_m(t)$ is the unit step signal which is defined as

$$U_m(t) = \begin{cases} +1, & \text{if } 0.2\,\text{s} < t < 0.4\,\text{s} \\ -1, & \text{if } 0.6\,\text{s} < t < 0.8\,\text{s} \\ 0, & \text{otherwise} \end{cases} \tag{19}$$

The DFT-based phasor estimation algorithm is applied to signal in Eq. (18) to compute the fundamental magnitude and phase angle. The performance during the above scenario under different sampling frequencies, i.e., $N \in \{64, 128, 256, 2048\}$ is depicted in Fig. 18. Its capacity during step change events is summarized in Table 5.

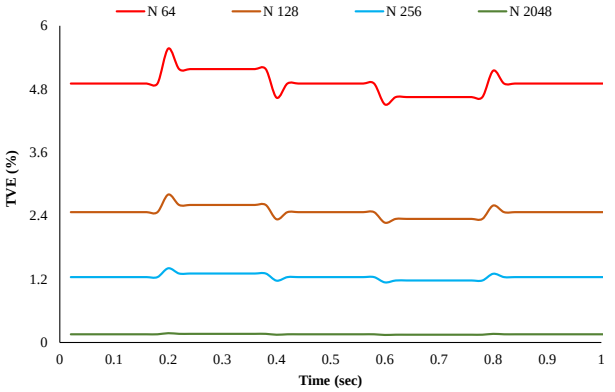

Fig. 18: *TVE response of Eq. (18) under step changes according to the IEEE C37.118.1a-2014 standard.*

Table 5: *Effect of sample rate during step change.*

N	% TVE		
	Maximum	Minimum	Mean
64	5.5692	4.5095	4.9109
128	2.8029	2.2696	2.4718
256	1.4059	1.1385	1.2399
2048	0.1762	0.1427	0.1554

Fig. 18 shows a peak and dip in TVE response at the instant of a positive and negative step change, respectively. The magnitude of peak and dip values reduces with an increase in sampling frequency during the phasor estimation process, as shown in Table 5. Furthermore, the step change in the signal has no impact, i.e., 0.1552% on TVE response during a sampling frequency of 2048 spc.

3.4.2 Interleave analysis during a step change event

An interleave analysis is performed to showcase the efficacy of the DFT-based phasor estimation algorithm during step change events. A 20 ms window shifted at a rate of five samples along with the signal in Eq. (18). Under different sampling frequencies, i.e., $N \in \{64, 2048\}$, the interleave analysis simulation results are depicted in Figs. 19 and 20, respectively. It can be observed that the TVE increases abruptly in the event of a step change, irrespective of its nature, i.e., either positive or negative, and the sampling frequency rate during the phasor estimation process. The simulation results reveal that the TVE exhibits an oscillating behavior response at around 5% and 0.162% TVE at 64 spc and 2048 spc, respectively. Furthermore, these oscillations reduced with an increase in sampling frequency rate during interleave analysis. The complete interleave analysis under various sampling frequencies is summarized in Table 6.

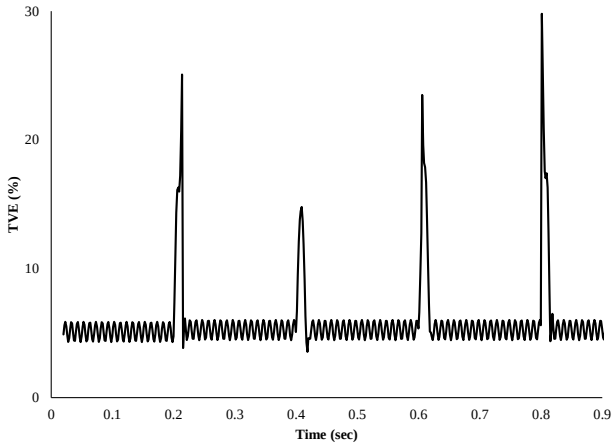

***Fig. 19**: TVE response during interleave analysis of Eq. (18) under 64 spc.*

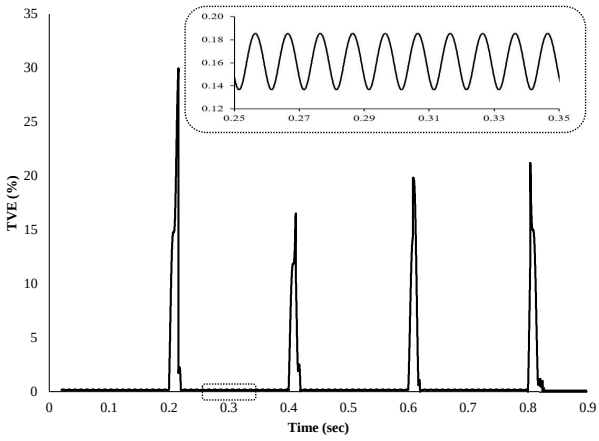

***Fig. 20**: TVE response during interleave analysis of Eq. (18) under 2048 spc.*

In addition, it can be observed from Fig. 21 that the TVE response is almost constant over time for Eq. (18) with DFT- based phasor estimation, displaying a magnitude of 0.15%. Whereas with SEM and LEM, the TVE response is purely constant with 1.77% and 2.91%.

3.4.3 Exponential decaying event

Due to the self-healing nature of an extensive interconnected power system, exponential dc decaying behavior of voltage/current signals arises during short circuit faults and the maloperation of relays and circuit breakers. Mathematically, these exponential dc decaying components in the voltage/current signal can be represented as

$$q_7(t) = Q_m \sin\left(2\pi f_0 t + \theta\right) + \gamma e^{(-t/\tau)} \qquad (20)$$

where γ is initial decaying magnitude i.e., 200 V, τ is time constant, i.e., 50 ms.

The TVE is computed by feeding the signal in Eq. (20) into the DFT-based phasor estimation algorithm to

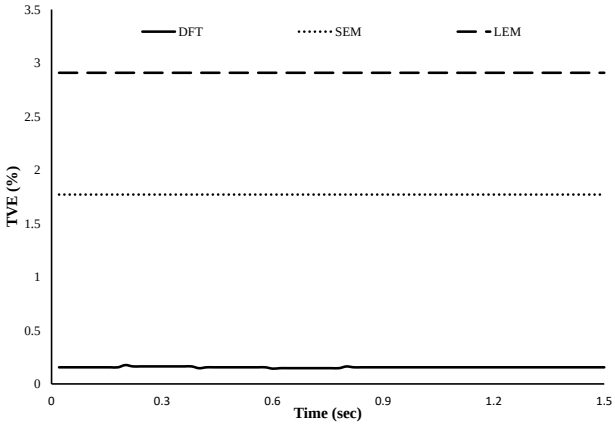

***Fig. 21**: TVE response of Eq. (18) under positive and negative step changes with DFT, SEM, and LEM.*

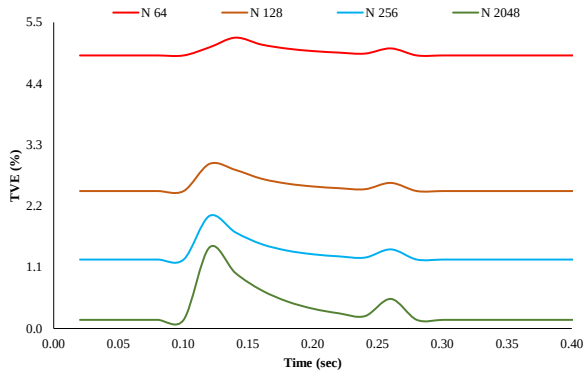

***Fig. 22**: TVE response of a sinusoidal signal with the magnitude exponential decaying with a change in time.*

***Table 6**: Maximum %TVE during interleave analysis of Eq. (18), i.e., step change scenario.*

N	% TVE at time t			
	0.2 s	0.4 s	0.6 s	0.8 s
64	25.0762	14.7985	23.4944	29.7951
128	28.7026	16.0943	18.9157	20.3747
256	29.0146	14.0825	19.2634	24.7451
2048	29.9025	16.5054	19.8205	21.0631

extract the fundamental magnitude and phase angle. The capacity of the DFT algorithm during the above scenario is shown in Fig. 22.

Fig. 22 reveals that the DFT-based estimation algorithm fails to extract sufficient fundamental phasor information during an exponentially dc decaying scenario with a sampling rate of 64 spc. Moreover, the accuracy of DFT algorithm is enhanced with an increase in the sampling rate, i.e., 128 spc, 256 spc. Under the above scenarios, the maximum TVE of 2.9580% and 2.0240% is attained with 128 spc and 256 spc sampling rates, respectively, during the phasor estimation process.

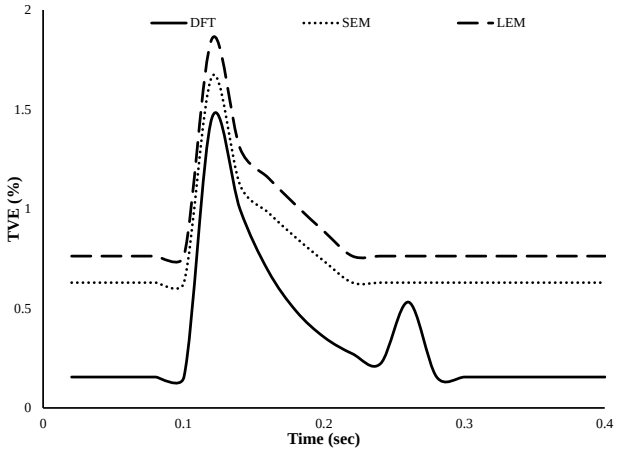

Fig. 23: *TVE response of Eq. (20) under DFT, SEM, and LEM phasor estimation techniques.*

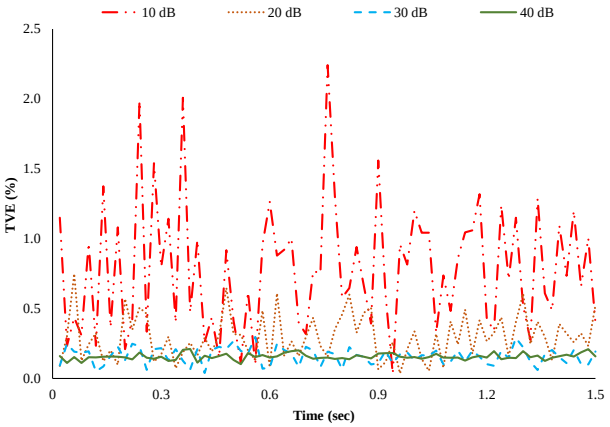

Fig. 24: *TVE response of Eq. (21) with a 30 dB noisy signal during a change in phase.*

Furthermore, the exact dynamics of the TVE response in synchronization with signal in Eq. (20) are exhibited by DFT-based phasor estimation with an accuracy of TVE $<$ 1% under a high sampling frequency rate, i.e., 2048 spc.

The TVE response conveyed in Fig. 23 follows the input signal over time for Eq. (20) with DFT-based phasor estimation displaying an average TVE of 0.34%. Whereas SEM and LEM provide an average TVE of 0.74% and 0.88%, respectively.

3.5 Signal with Random Abnormality

Electrical noise is an unwanted signal caused by loose transmission connections and distribution lines near the circuit breaker, downed power electronic devices, abnormal tuned capacitor banks, corona discharge lines, etc. Noise transmits into the power system, which may destroy the shape of the original signal, mathematically represented as

$$q_8(t) = Q_m \sin\left(2\pi f_0 t + \theta\right) + \chi \qquad (21)$$

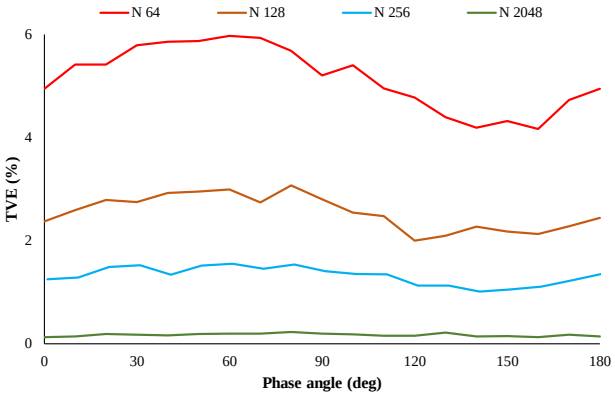

Fig. 25: *TVE response of Eq. (21) under the 30 dB noise scenario in the time domain.*

Table 7: *Results from Figs. 24 and 25.*

	% TVE					
	$\theta = 0$–180°			$t = 0$–1.5 s		
N	Maximum	Minimum	Mean	Maximum	Minimum	Mean
64	5.9715	5.3905	4.1659	12.5138	6.1567	2.1310
128	3.0713	2.5476	1.9997	9.3612	3.4288	0.2930
256	1.5359	1.3202	1.1027	4.5412	2.0199	0.4434
2048	0.2160	0.1718	0.1284	1.5703	0.6195	0.1140

where χ is the signal to noise ratio (SNR).

The signal in Eq. (21) with an SNR of 30 dB is given to the DFT-based phasor estimation algorithm to showcase its strength by changing the phase angle (θ) from 0° to 180° with a step size of 10° at fixed magnitude (Q_m) under different sampling frequencies, i.e., $N \in \{64, 128, 256, 2048\}$ as shown in Fig. 24. Furthermore, the strength of DFT during the phasor estimation of Eq. (21) is depicted in Fig. 25 under different sampling frequencies, i.e., $N \in \{64, 128, 256, 2048\}$ and its efficacy summarized in Table 7.

The simulation results reveal that an accuracy of TVE $<$ 3% is achieved during the phasor estimation of Eq. (21) with an SNR of 30 dB during sampling frequencies, i.e., $N > 128$ spc. Moreover, the DFT-based phasor estimation is immune (i.e., mean TVE of 0.62% at an SNR of 30 dB) to noise at very high sampling frequency rates, i.e., 2048 spc, as shown in Fig. 25. Table 7 clearly shows that TVE reduces with high sampling frequencies, i.e., N.

Furthermore, the performance of DFT-based estimation algorithm is explored by varying the SNR from 10 dB to 40 dB under a sampling rate of 2048 spc, and the corresponding simulation results are shown in Fig. 26.

It can be observed from Fig. 26 that DFT can extract the fundamental phasor efficiently with TVE according to the IEEE C37.118.1a-2014 standard (i.e., less than 3%) with a minimum sampling frequency of 2048 spc. Furthermore, the accuracy of the DFT algorithm exceeds 3% during the noise scenario with an SNR of less than

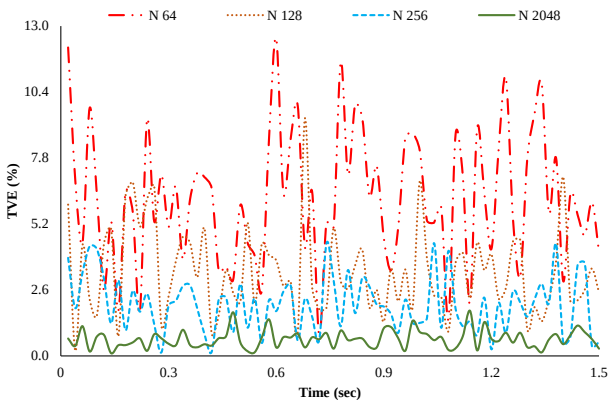

***Fig. 26**: TVE response of Eq. (21) for DFT with SNR varying noise levels.*

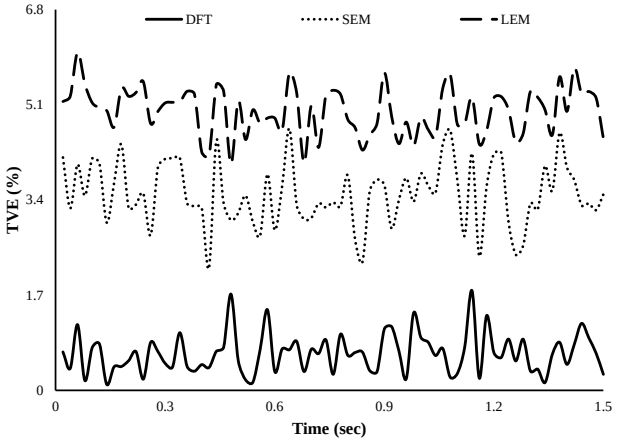

***Fig. 27**: TVE response of Eq. (21) under the random noise scenario with DFT, SEM, and LEM phasor techniques.*

7 dB, which is not acceptable. Thus, the DFT-based phasor estimation algorithm with a high sampling rate, i.e., $N \geq 2048$ spc can accurately extract the fundamental phasor (i.e., maximum of TVE up to 3%) in noisy scenarios with an SNR > 10 dB.

Moreover, Fig. 27 reveals that the TVE response is irregular over time for Eq. (21) with DFT-based phasor estimation with an average magnitude of 0.66%. Whereas with SEM and LEM the TVE response is 3.50% and 4.98%, respectively.

4. CONCLUSION

This paper provides an in-depth analysis of dynamic phasor estimation based on DFT with various ADC sampling rates and validated under the test signals provided by the IEEE C37.118.1a-2014 standard. The in-depth analysis of the DFT-based phasor estimation algorithm has been carried out by varying the phase angle (i.e., 0° to 180°) of a signal and estimated window length (i.e., 20 ms and 5 ms). Furthermore, the DFT-based phasor estimation with a sampling frequency of 2048 was compared with the SEM and LEM using a sampling frequency of 128.

The simulation results reveal that the efficacy (%TVE) of phasor estimation increases along with the sampling frequency (i.e., <10% for 64, <5% for 128, <2.5% for 256, and <1% for 2048) of an analog to digital converter (ADC) during various dynamic scenarios except for adverse frequency ramp events. The DFT algorithm with a very high sampling rate can be immune to noise levels up to an SNR of 10 dB. Furthermore, an ADC with 2048 spc is required to achieve <1% TVE accuracy during dynamic phasor estimation through DFT. According to a comparative analysis of the DFT-based estimation analysis, SEM, and LEM, it is clear that the TVE response of the DFT-based estimation algorithm follows the signal behavior for almost all test signals. In contrast, the SEM and LEM fail to perform satisfactorily in the frequency ramp, step change, and exponential decaying events.

Thus, the results presented in this paper demonstrate that DFT-based dynamic phasor estimation algorithms have the necessary capacity to develop PMUs for wide-area monitoring and the control of smart electric grids.

REFERENCES

[1] N. Hatziargyriou, H. Asano, R. Iravani, and C. Marnay, "Microgrids," *IEEE Power and Energy Magazine*, vol. 5, no. 4, pp. 78–94, Jul. 2007.

[2] R. Lasseter and P. Paigi, "Microgrid: a conceptual solution," in *2004 IEEE 35th Annual Power Electronics Specialists Conference*, Aachen, Germany, 2004, pp. 4285–4290.

[3] S. Vijayalakshmi and D. Kavitha, "Optimal placement of phasor measurement units for smart grid applications," in *2018 National Power Engineering Conference (NPEC)*, Madurai, India, 2018.

[4] R. Dugan and S. Price, "Issues for distributed generation in the US," in *2002 IEEE Power Engineering Society Winter Meeting*, New York, New York, USA, 2002, pp. 121–126.

[5] *IEEE Standard for Synchrophasor Measurements for Power Systems – Amendment 1: Modification of Selected Performance Requirements*, IEEE Std C37.118.1a-2014 (Amendment to IEEE Std C37.118.1-2011), Apr. 2014.

[6] *IEEE Standard for Synchrophasor Measurements for Power Systems*, IEEE Std C37.118.1-2011, Dec. 2011.

[7] M. Wang and Y. Sun, "A practical method to improve phasor and power measurement accuracy of DFT algorithm," *IEEE Transactions on Power Delivery*, vol. 21, no. 3, pp. 1054–1062, Jul. 2006.

[8] J.-W. Choi, Y.-K. Kim, and H.-G. Kim, "Digital PLL control for single-phase photovoltaic system," *IEE Proceedings - Electric Power Applications*, vol. 153, no. 1, pp. 40–46, Jan. 2006.

[9] B. Khettaoui and M. Boudour, "Synchrophsor estimation based on the combination of the modulated sliding DFT and Taylor's series expansion," in *2018*

International Conference on Electrical Sciences and Technologies in Maghreb (CISTEM), Algiers, Algeria, 2018.

[10] B. Kim, S.-H. Kong, and S. Kim, "Low computational enhancement of STFT-based parameter estimation," *IEEE Journal of Selected Topics in Signal Processing*, vol. 9, no. 8, pp. 1610–1619, Dec. 2015.

[11] D. Belega and D. Petri, "Fast Taylor weighted least squares algorithm for synchrophasor estimation," in *2019 IEEE 5th International forum on Research and Technology for Society and Industry (RTSI)*, Florence, Italy, 2019.

[12] D. Belega and D. Petri, "Effect of windowing and noise on the amplitude and phase estimators returned by the taylor-based weighted least squares," *Digital Signal Processing*, vol. 83, pp. 202–213, Dec. 2018.

[13] D. Macii and D. Petri, "A simple time-domain algorithm for synchrophasor, frequency and ROCOF estimation," in *2019 IEEE International Instrumentation and Measurement Technology Conference (I2MTC)*, Auckland, New Zealand, 2019.

[14] M. Perez, J. Espinoza, L. Moran, M. Torres, and E. Araya, "A robust phase-locked loop algorithm to synchronize static-power converters with polluted AC systems," *IEEE Transactions on Industrial Electronics*, vol. 55, no. 5, pp. 2185–2192, May 2008.

[15] D. Yazdani, A. Bakhshai, and P. K. Jain, "A three-phase adaptive notch filter-based approach to harmonic/reactive current extraction and harmonic decomposition," *IEEE Transactions on Power Electronics*, vol. 25, no. 4, pp. 914–923, Apr. 2010.

[16] A. Nicastri and A. Nagliero, "Comparison and evaluation of the PLL techniques for the design of the grid-connected inverter systems," in *2010 IEEE International Symposium on Industrial Electronics*, Bari, Italy, 2010, pp. 3865–3870.

[17] S. Toscani, C. Muscas, and P. A. Pegoraro, "Design and performance prediction of space vector-based PMU algorithms," *IEEE Transactions on Instrumentation and Measurement*, vol. 66, no. 3, pp. 394–404, Mar. 2017.

[18] S. Affijulla and P. Tripathy, "Development of phasor estimation algorithm for P-class PMU suitable in protection applications," *IEEE Transactions on Smart Grid*, vol. 9, no. 2, pp. 1250–1260, Mar. 2018.

[19] S. Affijulla and P. Tripathy, "Development of dictionary-based phasor estimator suitable for P-class phasor measurement unit," *IEEE Transactions on Instrumentation and Measurement*, vol. 67, no. 11, pp. 2603–2615, Nov. 2018.

[20] K. Chauhan, M. V. Reddy, and R. Sodhi, "A novel distribution-level phasor estimation algorithm using empirical wavelet transform," *IEEE Transactions on Industrial Electronics*, vol. 65, no. 10, pp. 7984–7995, Oct. 2018.

[21] A. Ashrafian, M. Mirsalim, and M. A. S. Masoum, "An adaptive recursive wavelet based algorithm for real-time measurement of power system variables during off-nominal frequency conditions," *IEEE Transactions on Industrial Informatics*, vol. 14, no. 3, pp. 818–828, Mar. 2018.

[22] K. Narendra, D. R. Gurusinghe, and A. D. Rajapakse, "Dynamic performance evaluation and testing of phasor measurement unit (PMU) as per IEEE C37.118.1 standard," in *Doble Client Committee Meetings & International Protection Testing Users Group (PTUG)*, Chicago, Illinois, USA, 2012.

[23] A. T. Munoz and J. A. de la O. Serna, "Shanks' method for dynamic phasor estimation," *IEEE Transactions on Instrumentation and Measurement*, vol. 57, no. 4, pp. 813–819, Apr. 2008.

[24] D. Belega, D. Fontanelli, and D. Petri, "Low-complexity least-squares dynamic synchrophasor estimation based on the discrete Fourier transform," *IEEE Transactions on Instrumentation and Measurement*, vol. 64, no. 12, pp. 3284–3296, Dec. 2015.

Sai Lakshmi Chukkaluru received the B.Tech. degree in Electrical and Electronics Engineering from Jawaharlal Nehru Technological University Kakinada, India, in 2018 and the M.Tech. degree in Power and Energy Systems from the National Institute of Technology Meghalaya, India in 2021. She is currently a Junior Research Fellow at the Indian Institute of Technology Palakkad, India. Her current research interests include synchrophasor technology in monitoring of wide area power systems.

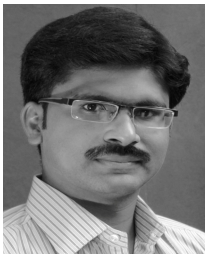

Shaik Affijulla received the M.Tech. degree in Electrical Engineering from National Institute of Technology Hamirpur, Himachal Pradesh, India in 2011 and Ph.D. degree in Electrical Engineering from National Institute of Technology Meghalaya, Shillong, India in 2018. Currently, he is working as Assistant Professor in the Department of Electrical Engineering at the National Institute of Technology Meghalaya, Shillong, India. His current research interests include the PMU estimation algorithms, application of Phasor Measurement Units for wide area protection and power system dynamics.